EUROSUN2026

Industrial steam supplied by a hybrid solar thermal-photovoltaic system

Giorgos Papakokkinos[1,*], Alaric Montenon[1,2], Petros Petrou[3], Maria Papadimitriou[3], Valéry Vuillerme[4]
[1]Energy, Environment and Water Research Center (EEWRC), The Cyprus Institute, Nicosia, Cyprus
[2]EPF School of Engineering, Montpellier, France
[3]Petrou Bros Dairy Products, Larnaca, Cyprus
[4]Univ. Grenoble Alpes, CEA, LITEN, DTCH, L2TS, Grenoble, France
*Email: g.papakokkinos@cyi.ac.cy

Summary

Solar technologies are expected to contribute to the decarbonization of industrial heat. Hybrid systems leverage the individual advantages of each technology, while benefiting from their synergy. A hybrid solar thermal-photovoltaic system is presented, which supplies heat to a dairy industry, in the form of saturated steam at 175 °C. A field of parabolic trough collectors is connected sequentially with a PV-fed electric heater. The integration approach of the hybrid system is highly case-specific, as it depends on the thermal load profile, as well as the existing energy sources and their constraints. Alongside a fossil fuel, a circular sustainable fuel is used, an in-house generated biogas with specific storage capacity, as well as generation and consumption rates. From environmental and economic perspectives, the biogas consumption is prioritized. The study employs a transient simulation model, developed using the Modelica language. Aligned with the decarbonization objective, the incorporation of the solar system decreases the fuels' consumption, with a more drastic reduction for the fossil fuel. The solar contribution is based on 82% solar thermal and 18% photovoltaic. The monthly contribution exhibits a high non-uniformity throughout the year, as the highest month contributes 5.5 times more heat than the lowest month. The investigation of a key design parameter, the outlet temperature of the solar thermal field, reveals its impact on the performance of the system. A scalability study investigates the influence of the field size on the fuel consumption and the appearance of curtailed heat.

Keywords: heat decarbonization, industrial heat, hybrid solar, concentrating solar
Field of application for the findings: Industrial heat, Concentrating Solar Heat
Addressed audience: researchers, engineers, industrial stakeholders

1 Introduction

Despite the recent progress in the penetration of Renewable Energy Sources (RES) in the electricity generation [1], industrial heat remains heavily dependent on fossil fuels. According to the International Energy Agency (IEA), the RES share in the global industrial heat consumption in 2024 was only 12% [2]. This corresponds to a considerable decarbonization potential, taking into consideration that industrial heat represents 26% of the total global energy consumption [3]. Concentrating Solar Thermal (CST) technologies are identified by IEA as a promising RES for contributing to the decarbonization of heat up to temperatures of 400 °C [4]. Moreover, IEA highlights that important benefits are also expected from the electrification of low-temperature heat and steam, along with the increasing RES penetration in electricity grids [5]. Photovoltaics (PV) can contribute to the heating of the heat transfer fluid or heat storage medium, through electrical resistances, induction devices or heat pumps. Therefore, both solar technologies can contribute to the decarbonization of industrial heat. Hybridization of the two solar technologies allows to take advantage of the individual benefits of each, as well as to create synergies among them. CST technologies have typically higher solar-to-heat conversion efficiency than PV [6]. PV have higher versatility and lower structural requirements with respect to the potential installation sites, as well as they benefit from both direct and diffuse radiation. An extensive discussion on this topic can be found in [6]. The authors of the latter review conclude that there are few studies about hybrid systems that specifically focus on industrial applications.

Rosales-Pérez et al. [7] studied the techno-economic performance of ST-PV systems. They developed a design methodology for ST-PV hybrid systems in series, for the evaluation of the performance of different scenarios in terms of solar fraction and Levelized Cost Of Heat (LCOH). Their results show that hybrid ST-PV systems achieve significant reductions in LCOH, compared to single-technology configurations. Moreover, they demonstrate that ST-PV systems perform better in solar fractions above 0.3, low and medium temperatures, and medium to high solar radiation potential. Saini et al. [8] investigated a hybrid ST-PV concept for steam production in the food and beverage industry. The system employs parabolic trough collectors with pressurized water thermal storage, alongside a PV-driven high-temperature sand storage. The authors report that the hybrid system exhibits an improved economic and land use performance, compared to the individual cases. The proposed system achieves a solar fraction of 90% and a 16% cost reduction compared to a boiler-based system. Sturm et al. [9] studied the integration of solar heat generation in a medium-sized condiment industry in China. They economically assessed flat plate solar collectors and PV-driven heat individually for hot water production. The single-technology configurations, as well as their combination in a hybrid cascade configuration, were also assessed for steam generation. In the latter, the hybrid cascade system was found to be the most economic option. Mousa et al. [10] performed multi-objective optimization studies of hybrid ST-PV systems for industrial applications. The two technologies operated in parallel, unlike the sequential configurations mentioned earlier. They used objective functions from economic, technical and environmental perspectives, based on the levelized cost, the overall performance and the embodied emissions, respectively. Their findings demonstrate that generally, the hybrid systems exhibit an improved performance to the single-technology configurations. The optimal technology mix was found to vary significantly across the 12 locations that were studied. Famiglietti and Abbas [11] considered the supply of $8\,\mathrm{bar}$ steam for industrial usage, generated by linear Fresnel collectors and by PV-driven high-temperature heat pumps, as well as by their hybrid combination in a parallel configuration. Colombi et al. [12] studied the decarbonization of medium-high temperature industrial heat ($300\,^{\circ}\mathrm{C}$ - $500\,^{\circ}\mathrm{C}$) by hybridizing CST with RES electric heating, the latter supplied by PV or wind energy. The system design and the hourly operation are optimized based on the metrics of LCOH and the cost of avoided $\mathrm{CO_2}$. Among other, the study investigated the influence of 3 different locations, the supplied temperature level, the collector orientation and the renewable penetration level.

The integration scheme of solar technologies in industrial processes is also an important aspect. Fuentes et al. [13] underline the lack of consensus regarding integration schemes for solar heat in the dairy industry. In their study, they assessed four types of solar thermal collectors in three Chilean locations with distinct solar potential. For their analysis, they performed annual transient simulations using the TRNSYS software. The selected integration scheme involves the utilization of solar heat to preheat the feedwater prior its entrance to the boiler. Among their conclusions is the determining impact of the integration scheme, which in this case limits the maximum solar energy supply to 10% of the total plant requirement. Rodríguez Rodrigo et al. [14] investigated the potential contribution of solar heat in dairy industries, by comparing parabolic trough and linear Fresnel collectors from technical and economic perspectives for 8 climatic zones. They have analyzed two representative dairy industry sizes for Spain with annual heat demand of $10\,\mathrm{GWh}$ and $60\,\mathrm{GWh}$. Integration studies are highly benefited by transient modeling, as the latter allow to study and develop integration concepts, operating strategies and control schemes that maximize the potential of solar technologies. Immonen et al. [15] simulated a $27\,\mathrm{MW_{th}}$ CST system for industrial process heat in the temperature range of $250\,^{\circ}\mathrm{C}$-$390\,^{\circ}\mathrm{C}$, using Simulink software. They proposed a flexible heat integration scheme and compared it with a base case. The optimized flexible integration exhibited an increase of 13% in the solar share and a 10.4% reduction in LCOH. Transient simulations were also performed by Crespo et al. [16] using the TRNSYS software, in order to simulate an existing PTC field in a grape juice industry, located in Chile. As reported, the solar field generated lower annual heat than expected. The study proposed integration scenarios for enhancing the performance of the system.

In the review of Rosales-Pérez et al. [6], it is concluded that further research is required on hybrid concepts, in order to analyze their performance under different temperatures, technologies combinations and solar potential characteristics. They also highlighted that the design and control of hybrid systems is more complex than conventional systems.

The present work studies the incorporation of a hybrid solar thermal-photovoltaic system in a dairy industry in Larnaca, Cyprus. In addition to the hybridization, the present study addresses another important aspect, the integration into the existing thermal system of an industry, which, as demonstrated, is highly case-specific in terms of thermal load profile and available energy sources. In this particular case, the case-specific nature of the integration is determined by the current utilization of a fossil fuel and a sustainable fuel with specific storage capacity, as well as consumption and generation rates. The objective is to quantify the contribution of the hybrid system and investigate the influence of key design parameters on its performance and integration into the existing industrial thermal system. Section 2 presents the thermal system and the heat load profile of the case study, as it was characterized within the Horizon project INDHEAP. Subsequently, the hybrid system and the integration concept are explained, followed by the presentation of the transient computational model that has been developed in order to perform the simulations. In Section 3, the base case is defined and studied.

The simulations allow the quantification of the solar share of the total consumption, the CST share within the solar contribution, their monthly distribution, the influence of the CST outlet temperature and the parametric study of the CST field size, providing insight into the performance and design implications of the proposed hybrid integration.

2 Methodology

2.1 Case study

The industrial case study under consideration is the dairy industry Petrou Bros Dairy Products (PBDP), located in Larnaca, Cyprus. This study is based on the thermal load profile of PBDP, as it was characterized within the INDHEAP project in 2025. The main heat consumers are cheese cooking (cheese in boiling liquid) and milk pasteurization. The heat produced to satisfy this demand is in the form of saturated steam at $8\,\mathrm{bar_g}$, at approximately $175\,°\mathrm{C}$. The required steam is produced by two boilers; one consumes exclusively Light Fuel Oil (LFO) and the other consumes alternately LFO and biogas. The biogas is generated on-site based on whey, a liquid by-product of the cheese production of PBDP. The steam is utilized both indirectly and directly. Indirect usage involves the steam condensation for providing the associated exothermic heat to the process through a heat exchanger, and its subsequent return to the boilers' block as liquid water at $80\,°\mathrm{C}$. Direct usage pertains to the steam injection directly inside the thermal process, without the possibility of recovering it. Consequently, water from the grid is replaced to compensate for the direct steam consumption, as well as for the water losses and the occasional boiler blowdown (water rejection to remove impurities). The replacement water is heated from the grid temperature to $70\,°\mathrm{C}$ using a Combined Heat and Power unit, which consumes primarily the in-house biogas. During nominal operation between 04:00 and 14:00, the steam generation is $5000\,\mathrm{kg/h}$ corresponding to a thermal load of $3.42\,\mathrm{MW}$. Between 14:00 and 17:00, a partial load of $1.8\,\mathrm{MW}$ takes place. This typical daily profile is repeated 5 or 6 days per week depending on the season. Figure 1 illustrates a schematic diagram of the thermal system of PBDP.

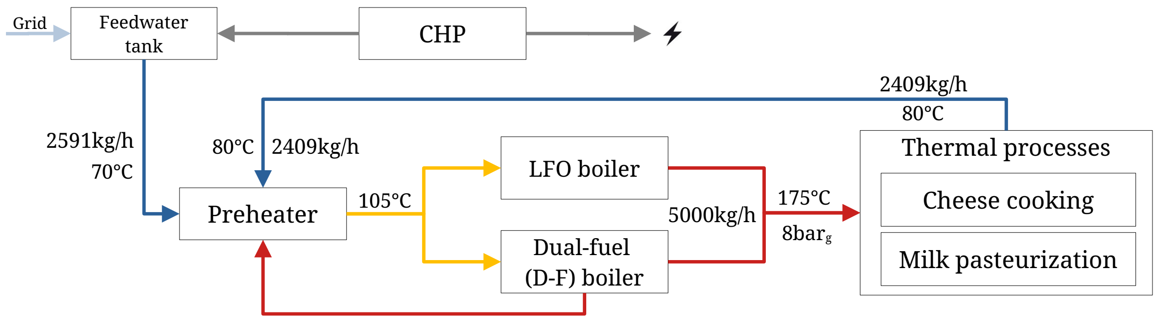

Figure 1: Schematic diagram of PBDP thermal system

An important aspect in the thermal system of PBDP is the management of the biogas. During operation, its consumption rate exceeds its generation rate, thus its storage is emptied and the dual-fuel boiler switches from biogas to LFO, in order to allow time for the biogas level to recover. In contrary, when no operation takes place, its generation rate is high enough to fill the existing storage, and the newly generated biogas is rejected. To avoid this, the aforementioned CHP unit consumes biogas during part of the boilers' downtime (17:00-24:00), in order to increase the feedwater tank temperature as mentioned earlier. Figure 2 shows the typical daily thermal load of PBDP, according to the boiler and the fuel.

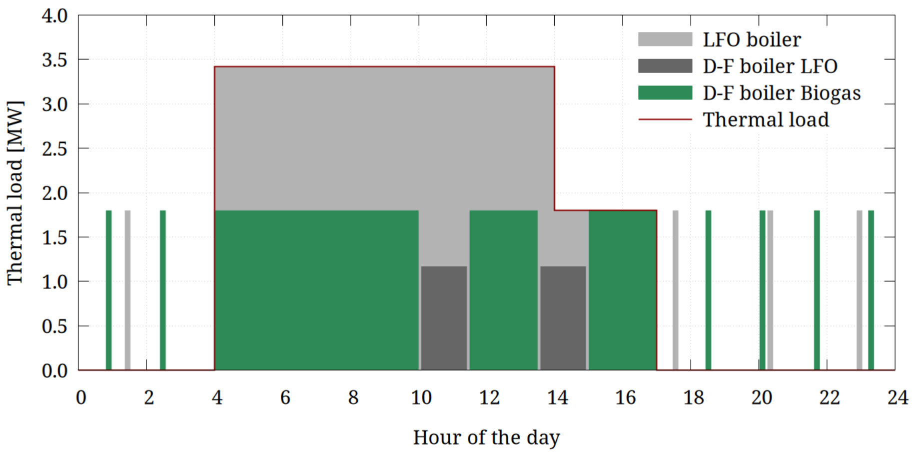

Figure 2: Typical daily thermal profile of PBDP according to boiler and fuel

2.2 Hybrid integration concept

The proposed integration concept involves the hybridization of the two solar technologies, CST and PV, in order to take advantage of their individual benefits. For the utilization of the electricity generated by the PV, an electric heater (e-heater) is employed. This PV-fed e-heater is connected in series with the CST field, and serves as a booster, to further elevate the temperature of the Heat Transfer Fluid (HTF). The solar HTF subsequently provides its heat for steam generation through two heat exchangers. The hybrid solar system is incorporated in parallel to the existing boilers' block and thus, it provides the same grade of steam, as opposed to a preheating configuration. The returning condensed water from the thermal processes along with the water from the feedwater tank are mixed and a three-way valve determines the flow distribution towards the boilers' block and the hybrid solar system, according to the production of the latter. Since the considered solar HTF is pressurized water, the possibility of a direct integration was also elaborated. In this concept, instead of delivering the heat through heat exchangers, the produced hot pressurized water would enter a flash evaporator, where a fraction of it would evaporate at the desired pressure and provide the steam to the process, while the rest would return as liquid. This integration concept was rejected mainly because it requires food-grade components throughout the entire system. Figure 3 illustrates the proposed integration concept of the solar hybrid system.

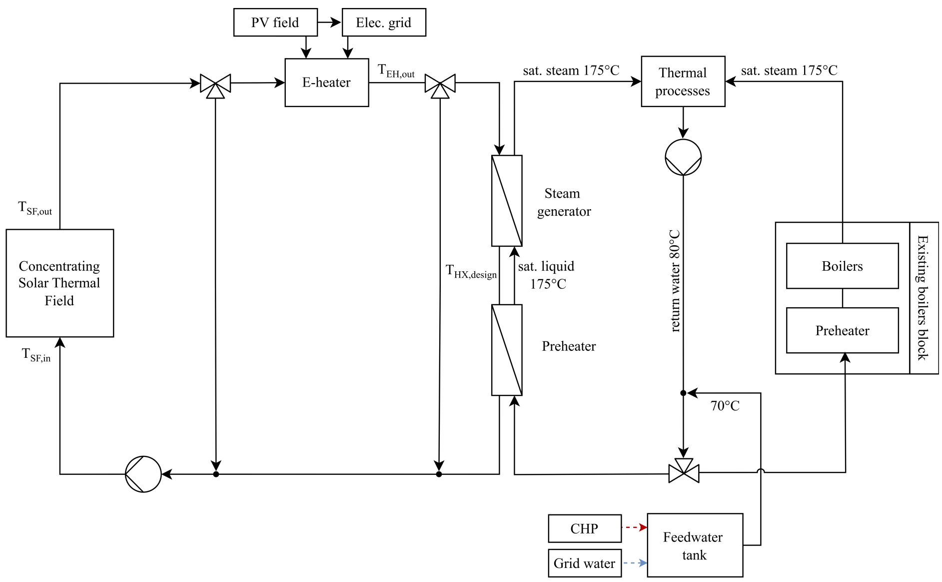

Figure 3: Schematic diagram of the proposed integration concept of the solar hybrid system

The base CST field is composed by 3 parallel subfields, each with 24 parabolic trough collectors connected in series. In the parametric study, multiples of this CST field are investigated. The solar loop interacts with the load loop through two heat exchangers, a preheater and a steam generator. The enthalpic levels on the load loop are determined by the thermal load, i.e. the return temperature is the mix of the two water streams (condensate and feedwater), the outlet of the preheater is saturated liquid at the corresponding load pressure and temperature ($8\,\mathrm{bar_g}$ and $175\,^\circ\mathrm{C}$), while the outlet of the steam generator is saturated steam at the aforementioned conditions. The CST field increases the temperature of the solar HTF from $180\,^\circ\mathrm{C}$ to $205\,^\circ\mathrm{C}$. The e-heater further elevates the HTF temperature to $210\,^\circ\mathrm{C}$, in order to allow higher temperature difference within the steam generator. The outlet temperature of the steam generator on the solar loop is a design parameter that has substantial influence on the heat exchangers' effectiveness, the ratio of the flow rates of the two loops, the CST/e-heater shares, and the solar field inlet temperature. Taking into consideration the above and the heat exchangers calculations, this temperature is set to $185\,^\circ\mathrm{C}$.

In this study, a heat storage unit has not been included. During operation, the heat produced by the solar hybrid system is considerably smaller than the thermal load of PBDP, thus it is completely absorbed and there is no excess heat to be stored. In the parametric study of the CST field size, it is shown that the excess heat appears only in large CST fields, when no space constraints are considered. Furthermore, during operating days there is no temporal mismatch to bridge between solar production and demand, since only 3% of the former lies outside the operating hours. This can be eliminated with a one-hour shift of the operating hours during some summer months, as an adaptation measure to the solar resource.

2.3 Computational model

For the simulation of the system, a transient computational model has been developed using the Modelica language [17], within the OpenModelica environment [18].

For the CST field, the performance of the parabolic trough collectors is described by the ISO 9806 standard [19]. The generated thermal power $\dot{Q}_{\mathrm{gen}}$ is calculated through the following equations, omitting the terms whose coefficient is zero for this particular collector. The mathematic formulation pertains to a north-south axis orientation and considers the shadow casted from adjacent collectors.

$$\dot{Q}_{\mathrm{gen}} = A_{\mathrm{col}} \left(\dot{q}_{\mathrm{abs}} - a_1 \left(T_{\mathrm{mf}} - T_{\mathrm{amb}}\right) - a_2 \left(T_{\mathrm{mf}} - T_{\mathrm{amb}}\right)^2 - a_5 \frac{dT_{\mathrm{mf}}}{dt} \right) \tag{1}$$

where:

$$\dot{q}_{\mathrm{abs}} = \eta_0 (I_{\mathrm{DNI}}\ \mathrm{IAM}(\theta_{\mathrm{L}}) \cos\theta_{\mathrm{L}}\ \eta_{\mathrm{shadow}} + I_{\mathrm{d}}\ \mathrm{IAM_d}) \tag{2}$$

where A_{col} is the collector area, η_0 is the optical efficiency, IAM denotes the Incidence Angle Modifiers and η_{shadow} represents the non-shaded portion of the collector surface; while the direct and diffuse solar irradiances I_{DNI} and I_{d} are imported from the weather file, and the longitudinal incident angle θ_{L} is calculated based on the solar position, i.e. the solar azimuth and elevation. The mean fluid temperature is calculated as $T_{\mathrm{mf}} = (T_{\mathrm{SF,in}} + T_{\mathrm{SF,out}})/2$. The flow rate of the CST field is calculated based on the generated heat, in order to achieve the setpoint of the outlet temperature of the CST field. The imposed flow rate is subjected to the operational limits, with minimum and maximum volumetric flow rates. The input parameters employed in equations 1 and 2 pertain to the characteristics of a PTC collector currently under product development; therefore, their numerical values are not publishable at this stage.

The electric heater is modeled as a transient lumped capacity component, as shown in equation 3. For its thermal inertia, a water volume of $200\,\mathrm{l}$ is considered, while for the calculation of its heat loss coefficient UA_{EH}, a cylindrical shape with height equal to its radius and an insulation with $10\,\mathrm{cm}$ thickness and conductivity of $0.05\,\mathrm{W/mK}$. It is equipped with an electrical resistance with maximum capacity of $100\,\mathrm{kW}$ for $\dot{Q}_{\mathrm{EH}}$ (for the base case and scaled in the parametric study of the CST field). The electric heater maintains its temperature at the designated temperature $210\,^\circ\mathrm{C}$ between 07:00 and 17:00. The flow rate is determined by the flow rate of the CST field.

$$\rho\, V_{\mathrm{EH}}\, c_p \frac{dT_{\mathrm{EH}}}{dt} = \dot{m}\, c_p \left(T_{\mathrm{SF,out}} - T_{\mathrm{EH}}\right) - UA_{\mathrm{EH}}(T_{\mathrm{EH}} - T_{\mathrm{amb}}) + \dot{Q}_{\mathrm{EH}} \tag{3}$$

The e-heater consumes electricity from the grid and from the PV production in a net metering scheme. The required PV field is calculated as the capacity that produces 10% more than the annual electricity consumption of the e-heater (an assumption to account for additional losses, e.g. inverter losses, downtime, soiling etc.). The annual production per m^2 of PV, in the location under consideration, is calculated based on a commercial product, taking into account the incident radiation on a tilted plane of $30°$ and south orientation, as well as a temperature-dependent efficiency [20].

$$\frac{P_{\text{PV}}}{A_{\text{PV}}} = \eta_{\text{PV}}(T)\, I_{\text{tilt}} \tag{4}$$

$$T_{\text{cell}} = T_{\text{amb}} + \frac{I_{\text{tilt}}}{800}\left(T_{\text{NOCT}} - 20\right)\left(1 - \frac{\eta_{\text{ref,PV}}}{\tau\alpha}\right)\frac{9.5}{5.7 + 3.8 v_{\text{wind}}} \tag{5}$$

$$\eta_{\text{PV}} = \eta_{\text{ref,PV}}\left[1 + \gamma\left(T_{\text{cell}} - T_{\text{ref}}\right)\right] \tag{6}$$

assuming a constant wind speed $v_{\text{wind}} = 1\,\text{m/s}$ and $\tau\alpha = 0.9$, while $\eta_{\text{ref,PV}}$, γ and T_{NOCT} pertain to a specific commercial PV panel and are obtained from [21].

The biogas storage level is also simulated dynamically as in equation 7, in order to determine when biogas is available or when the dual-fuel boiler has to switch to the LFO. When the biogas storage is depleted, a hysteresis is applied in order to allow the biogas level to recover. The model also quantifies the excess biogas which is rejected when the storage is full and cannot accommodate the newly generated biogas.

$$\frac{dV_{\text{biogas}}}{dt} = \dot{v}_{\text{generation}} - \dot{v}_{\text{consumption}} \tag{7}$$

The implemented plant operation scheme prioritizes the utilization of the solar and the biogas heat production. Consequently, the LFO consumption is adapted accordingly, in order to satisfy the total demand. For the input climate data, the Typical Meteorological Year (TMY) is used for the location under consideration, namely Larnaca, Cyprus [22]. For the input and processing of the TMY file and its content, the following classes from the Modelica Buildings Library were used: ReaderTMY3, SolarAzimuth, DirectTiltedSurface and CalendarTime [23]. All the other required models were developed in-house. The simulation timestep is $10\,\text{min}$, although smaller timesteps are used by Modelica when state events occur.

3 Results and discussion

The Reference Case (RC) pertains to the case without the contribution of the solar hybrid system, according to the characterized thermal profile. The operating days are 295 per year, amounting to a total heat consumption of $11.682\,\text{GWh}$. The fuels' share is $45.4\,\%$ for biogas and $54.6\,\%$ for LFO. As commented, the CST field of the Base Case (BC) is composed by 3 parallel subfields, each of them with 24 parabolic solar collectors connected in series. The contribution of each source for the reference case and the base case are summarized in the Table 1.

Table 1: Energy contribution and share of the different energy sources for the reference and base cases

	Reference case		Base case	
	Contribution [MWh]	Share [%]	Contribution [MWh]	Share [%]
Biogas	5298	45.4	5234	44.8
LFO	6384	54.6	6034	51.7
Hybrid solar	–	–	414	3.5
Total	11682	100	11682	100

In the reference case, the two fuels satisfy the entire demand. In the base case, the hybrid solar thermal-photovoltaic system contributes by 3.5% of the total demand. The contribution of the hybrid solar results in a decrease of the fuels' contribution. However, the reduction is not uniform among the two fuels. The LFO reduction is 5.5%, whereas the biogas reduction is 1.2%. From another perspective, the solar production of $414\,\text{MWh}$ displaced approximately $350\,\text{MWh}$ of LFO and $64\,\text{MWh}$ of biogas. Consequently, 84.5% of the solar contribution displaced LFO consumption, while the remaining 15.5% displaced biogas consumption. This is a desirable and sought effect, since as explained earlier, the biogas consumption is prioritized over the LFO consumption. This objective is beneficial from both decarbonization and economic perspectives, as it prioritizes the reduction of the purchased fossil-fuel which is also associated with greenhouse gas emissions, rather than the circular, in-house, sustainable fuel. Out of the $414\,\text{MWh}$ contributed by the hybrid solar system to the PBDP consumption, 82% is provided by the CST, while 18% is provided by the PV-fed e-heater. A steady-state share would correspond roughly to the designated temperature increase of each technology; in this case $25\,°C$ and $5\,°C$, respectively. The CST share is lower than its corresponding steady-state share. This reduction arises since there are intervals when the CST operates with a lower $T_{SF,out}$ than the designated setpoint ($205\,°C$ in the base case, its influence is elaborated later), so the e-heater contribution is higher in order to bring the HTF to the designated $T_{EH,out} = 210\,°C$. These intervals occur at the beginning and at the end of the day, when the CST field is preheating or cooling down. They also occur during intervals with insufficiently high irradiance, when even with the lowest volumetric flow rate, the setpoint of $T_{SF,out}$ cannot be achieved. This is also reflected in the monthly production that is elaborated later.

It is noted that the aforementioned e-heater share corresponds to the useful heat provided to the HTF. Its actual consumption is higher, considering that heat is provided to compensate for the thermal losses. The details of the calculation of its thermal losses (shape, insulation thickness and thermal conductivity) are reported in Section 2.3. In the base case, the e-heater useful contribution is $75.1\,\mathrm{MWh}$, while its consumption is 2.3% higher at $76.9\,\mathrm{MWh}$. As discussed, the PV field is sized in order to provide 10% more than the annual consumption of the e-heater. The relevant annual PV production is $363.9\,\mathrm{kWh/m^2}$, taking into consideration the TMY of the location under consideration, as well as the temperature-dependent efficiency of a commercial PV. The characteristics of the PV and its orientation are reported in Section 2.3. Consequently, the required PV area and peak capacity when rounded upwards to the nearest panel are $234\,\mathrm{m^2}$ and $45.4\,\mathrm{kW_p}$, respectively.

Figure 4 presents the monthly contribution of the hybrid solar system, based on each of the two technologies. As it can be observed, the solar contribution exhibits a significant non-uniformity throughout the year. The monthly contribution of the system ranges between $11\,\mathrm{MWh}$ in December and $60\,\mathrm{MWh}$ in July. Moreover, the CST share varies considerably between 74.8% in December and 84.7% for June. The lower values exhibited in winter are a consequence of more frequent intervals with insufficient solar radiation, and thus, the inability to achieve the setpoint even with the lowest volumetric flow rate. According to the earlier discussion regarding the steady-state CST share, the highest value implies that there are periods when the outlet temperature is higher than the setpoint, even at the highest volumetric flow rate. These variations in the performance of the CST field determine the energy input of the e-heater accordingly.

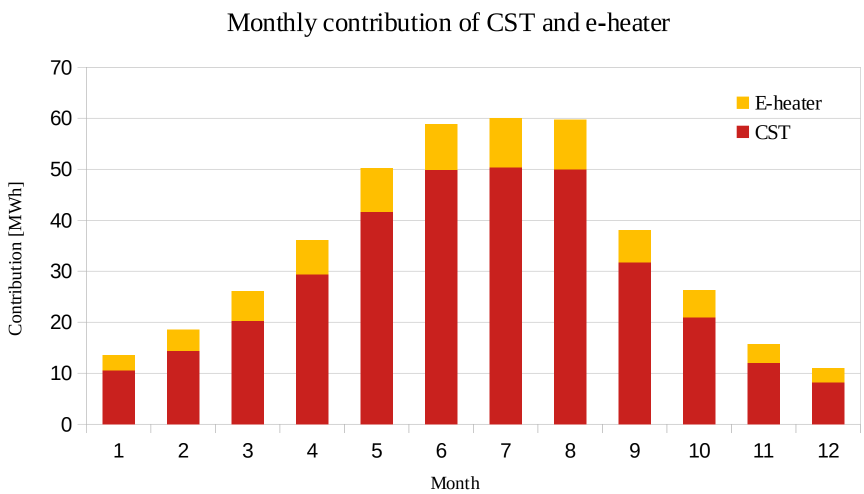

Figure 4: Monthly contribution of the hybrid system

The non-uniformity of the contribution of the system towards the load should be taken into consideration in several design and operational aspects. For the CST field, this is an intrinsic feature. However, the e-heater capacity remains underexploited for a big portion of the year. This encourages the possibility of repurposing the e-heater in other industrial processes, potentially taking advantage of the periods with low-cost grid electricity.

The base case considered $205\,°C$ as the outlet temperature of the CST and, consequently, the inlet to the e-heater. Subsequently, a sensitivity analysis of this design choice is presented, by modifying the $T_{SF,out}$ between $201\,°C$ and $207\,°C$ with a step of $2\,°C$. For a fixed $T_{EH,out} = 210\,°C$, the choice of $T_{SF,out}$ determines the heat provided by the CST field and the remaining heat provided by the e-heater. Table 2 summarizes the most relevant results. As it can be observed, increasing the $T_{SF,out}$ provokes a slight decrease in the CST contribution, since the latter is operated at higher temperatures and thus it has more heat losses. Also, as $T_{SF,out}$ increases, the required flow rate to achieve the setpoint is lower. Consequently, since the flow rate determines the total heat delivered to the load, the latter decreases as well. The total contribution of the hybrid system decreases from $461.3\,\mathrm{MWh}$ (for $201\,°\mathrm{C}$) to $387.2\,\mathrm{MWh}$ (for $207\,°\mathrm{C}$), a reduction of 16%, whereas the CST share increases from 73.7% (for $201\,°\mathrm{C}$) to 87.6% (for $207\,°\mathrm{C}$). Consequently, the contribution of the PV-fed e-heater decreases, and accordingly, the required PV field decreases from $72.4\,\mathrm{kW_p}$ to $29.6\,\mathrm{kW_p}$. Concluding, increasing $T_{\mathrm{SF,out}}$ increases the CST share but decreases the total heat provided by the hybrid system. These results pertain to a fixed $T_{\mathrm{SF,out}}$ throughout the year, but this could be variable, depending on the overall plant management supervisory control.

Table 2: Influence of the CST outlet temperature setpoint on the hybrid solar system

$T_{\mathrm{SF,out}}$	CST		PV-fed e-heater			Hybrid solar	
	Contribution [MWh]	Share [%]	E-heater consumption [MWh]	PV field [m^2]	PV capacity [kW$_p$]	Contribution [MWh]	Share [%]
201	339.8	73.7	123.3	373	72.4	461.3	3.95
203	339.5	77.3	101.4	308	59.7	439.2	3.76
205	339.3	81.9	76.9	234	45.4	414.4	3.55
207	339.0	87.6	49.9	153	29.6	387.2	3.31

Subsequently, the focus is shifted to the CST field size. The base case considered 3 parallel subfields, each with 24 collectors in series. Simulations with multiples up to 10x of the base CST field were performed. Figure 5 summarizes the share of each source (hybrid solar, biogas and LFO) with respect to the total load. Moreover it also presents the curtailed heat produced by the CST field during the operation hours (excluding non-operating hours and days). Curtailed CST heat is expressed as a percentage of the useful CST heat production. As it can be observed up to the multiple 6, the hybrid system contribution is absorbed completely and no excess production is rejected. As illustrated in the graph, the curtailed CST heat appears for the multiple of 7, with the rejected heat being 1.5 % of the useful CST production and increasing up to 7.8 % for the multiple of 10. Indicatively, the solar share for the base case is 3.5%, for the multiple 5 it is 17.7% and for the multiple of 10 it is 33.2%. Moreover as it can be observed from Figure 5, the prioritization of biogas consumption results in a higher decrease in the LFO consumption and lower decrease in biogas. Between the base case and multiple 10, the biogas share drops from 44.8% to 38.3%, whereas the LFO share experiences a drastic reduction from 51.7% to 28.5%. Consequently, the fuel share reduction for biogas and LFO is 6.5 and 23.1 percentage points, respectively.

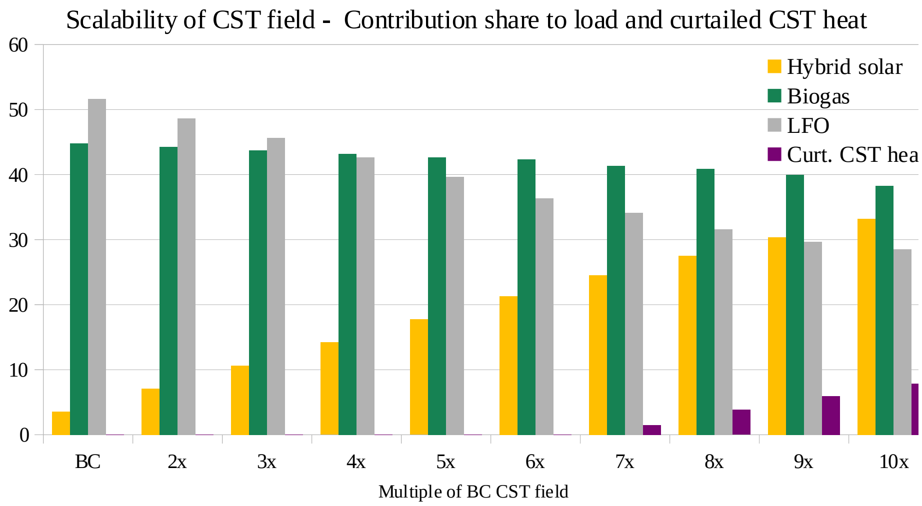

Figure 5: Share of contribution to the load by each source and curtailed CST heat as a percentage of useful CST heat production

4 Conclusions

A hybrid solar thermal-photovoltaic system has been proposed for the provision of process heat at a dairy industry in Larnaca, Cyprus. The heat is provided in the form of saturated steam at $8\,\mathrm{bar_g}$. The integration concept involves the CST field connected sequentially with an e-heater which elevates further the HTF temperature. Subsequently, the HTF provides heat to the load loop through a preheater and a steam generator. The dairy industry under consideration satisfied its heat demand through the combustion of a purchased fossil fuel, LFO, and an in-house biogas, generated on-site using a byproduct of its cheese production. Therefore, it was crucial that the hybrid solar contribution would displace primarily the fossil fuel rather than the sustainable, circular fuel.

For the numerical study, a transient model was developed using the Modelica language, taking into consideration the involved components. A base case has been defined and simulated. In this case, the contribution of the hybrid solar system was $414\,\mathrm{MWh}$, a solar share of 3.5%. The 84.5% of this contribution displaced LFO, while the remaining 15.5% displaced biogas. This is aligned with the overall objective of prioritizing the consumption of biogas. Within the hybrid solar contribution, the CST share was 82% and the required PV capacity to satisfy the annual demand of the e-heater was $45.4\,\mathrm{kW_p}$.

The influence of the outlet temperature of the CST field was studied and quantified, indicating the importance of such design choices. Increasing $T_{\mathrm{SF,out}}$ from $201\,^{\circ}\mathrm{C}$ to $207\,^{\circ}\mathrm{C}$ increased the CST share from 73.7% to 87.6%, while it decreased the total contribution of the system by 16%. These effects are direct consequences of the influence of the CST field flow rate on the performance of this hybrid concept.

The monthly distribution of the hybrid system was evaluated, revealing a substantial non-uniformity throughout the year. The system delivers to the load $11\,\mathrm{MWh}$ in December and $60\,\mathrm{MWh}$ in July. This significant discrepancy should be taken into consideration in the design stage of such systems. While for the CST this is an intrinsic characteristic arising from the seasonality of the solar potential, the capacity of the e-heater would remain underexploited during periods with low radiation. Therefore, identifying other usages of the e-heater is key, with a promising possibility being its utilization when grid electricity prices are low.

A parametric analysis of the CST field size was conducted, by considering multiples up to 10 with respect to the base case. According to the CST multiple, the solar share increased from 3.5% to 33.2%. This contribution resulted in a drastic decrease of the LFO consumption, decreasing its share from 51.7% to 28.5%. The decrease of biogas was moderate, as it was the objective, and its share decreased from 44.8% to 38.3%. Curtailed CST heat appeared at multiple 7, representing 1.5 % of the useful CST production and increased to 7.8 % for the multiple of 10. At those CST field sizes, the solar production is so high that cannot be completely absorbed by the load and the incorporation of thermal energy storage becomes relevant.

The study demonstrates the potential of incorporating a hybrid solar thermal-photovoltaic system for industrial heat. It also highlights the case-specific nature of such integration, which depends strongly on the industrial load profile, the available energy sources and their potential limitations, such as the storage capacity for biogas.

Two main directions are identified as future work. As demonstrated above, a thermal energy storage incorporation was not suitable for the daily operation and only becomes relevant for large CST fields. However, there are 70 non-operating days per year, being 1 or 2 each weekend. The potential CST production of those days was quantified as an additional 23.2% of the useful CST contribution. Exploiting this heat is expected to be beneficial for the levelized cost of heat of the system. Although a substantial heat amount, this production varies significantly among the weekends of the year. As it is also produced once a week, its integration is not straight-forward. The second future study is motivated by the space constraints within the premises of PBDP, while there is possibility to install the CST field off-site, in a nearby plot. Similar space constraints are expected to be a frequent bottleneck for the adoption of CST technologies in industrial sites. Consequently, future studies will focus on the effect of the off-site CST incorporation in terms of additional thermal losses as well as additional thermal mass.

Acknowledgments

This project has received funding from the European Union's Horizon Europe Research and Innovation Programme under Grant Agreement No 101136140. This project has received funding from the European Union's Horizon Europe research and innovation program under grant agreement No 101136140.

Nomenclature

Latin symbols

A	Area [m^2]
a_1	First-order heat loss coefficient [W/(m^2 K)]
a_2	Second-order heat loss coefficient [W/(m^2 K^2)]
a_5	Effective thermal capacity [J/(m^2 K)]
c_p	Specific heat capacity [J/(kg K)]
I	Solar irradiance [W/m^2]
$\dot{m}$	Mass flow rate [kg/s]
P	Electrical power [W]
$\dot{Q}$	Heat flow rate [W]
$\dot{q}$	Heat flux [W/m^2]
T	Temperature [$^\circ$C]
UA	Thermal transmittance [W/K]
V	Volume [m^3]
$\dot{v}$	Volumetric flow rate [m^3/s]

Subscripts

abs	Absorbed
amb	Ambient
col	Collector
d	Diffuse
gen	Generated
in	Inlet
mf	Mean fluid
out	Outlet
ref	Reference
tilt	Tilted surface

Greek symbols

γ	PV efficiency temperature coefficient [%/K]
η	Efficiency [-]
θ_L	Longitudinal incidence angle [$^\circ$]
ρ	Density [kg/m^3]

Abbreviations

BC	Base Case
CHP	Combined Heat and Power
CST	Concentrating Solar Thermal
DNI	Direct Normal Irradiance
EH	Electric heater
HTF	Heat Transfer Fluid
IAM	Incidence Angle Modifier
IEA	International Energy Agency
LFO	Light Fuel Oil
LCOH	Levelized Cost Of Heat
NOCT	Nominal Operating Cell Temperature
PBDP	Petrou Bros Dairy Products
PTC	Parabolic Trough Collectors
PV	Photovoltaic
RC	Reference Case
RES	Renewable Energy Sources
SF	Solar field
ST	Solar Thermal
TMY	Typical Meteorological Year

References

[1] International Energy Agency (IEA), Electricity – Global Energy Review 2025, IEA, Paris, 2025. `https://www.iea.org/reports/global-energy-review-2025/electricity` (accessed August 2026).

[2] International Energy Agency (IEA), *Renewables 2025*, IEA, Paris, 2025. `https://www.iea.org/reports/renewables-2025/renewable-heat`. (accessed August 2026).

[3] International Energy Agency (IEA), *Renewables 2025: Analysis and Forecasts to 2030*, IEA, Paris, 2025. `https://www.iea.org/reports/renewables-2025` (accessed August 2026).

[4] IEA Solar Heating and Cooling Programme, *Solar Heat for Industrial Processes (SHIP)*, Technology Position Paper, Task 64, 2024. `https://pubs.iea-shc.org/technology-position-papers` (accessed August 2026).

[5] International Energy Agency (IEA), *Renewables for Industry: Electrification of Low-Temperature Heat and Steam*, IEA, Paris, 2025. `https://www.iea.org/reports/renewables-for-industry` (accessed August 2026).

[6] J.F. Rosales-Pérez, A. Villarruel-Jaramillo, J.A. Romero-Ramos, M. Pérez-García, J.M. Cardemil, R. Escobar, Hybrid system of photovoltaic and solar thermal technologies for industrial process heat, *Energies* 16 (5) (2023) 2220. `https://doi.org/10.3390/en16052220`

[7] J.F. Rosales-Pérez, A. Villarruel-Jaramillo, M. Pérez-García, J.M. Cardemil, R. Escobar, Energy and economic performance evaluation of solar thermal and photovoltaic hybrid systems for industrial process heating, *Energy* 324 (2025) 135765. `https://doi.org/10.1016/j.energy.2025.135765`

[8] P. Saini, V. Kivioja, L. Naskali, J. Byström, C. Semeraro, A. Gambardella, X. Zhang, Techno-economic assessment of a novel hybrid system of solar thermal and photovoltaic driven sand storage for sustainable industrial steam production, *Energy Conversion and Management* 292 (2023) 117414. https://doi.org/10.1016/j.enconman.2023.117414

[9] B. Sturm, S. Meyers, Y. Zhang, R. Law, E.J. Siqueiros Valencia, H. Bao, Y. Wang, H. Chen, Process intensification and integration of solar heat generation in the Chinese condiment sector – A case study of a medium sized Beijing based factory, *Energy Conversion and Management* 106 (2015) 1295–1308. https://doi.org/10.1016/j.enconman.2015.10.045

[10] O. Bany Mousa, R.A. Taylor, A. Shirazi, Multi-objective optimization of solar photovoltaic and solar thermal collectors for industrial rooftop applications, *Energy Conversion and Management* 195 (2019) 392–408. https://doi.org/10.1016/j.enconman.2019.05.012

[11] A. Famiglietti, R. Abbas, Steam generation for industry using linear Fresnel solar collectors and PV-driven high-temperature heat pumps: Techno-economic analysis, *Solar* 5 (2) (2025) 27. https://doi.org/10.3390/solar5020027

[12] M. Colombi, P. Colbertaldo, M.C. Romano, M. Binotti, Industrial process heat decarbonisation with hybrid concentrated solar thermal and electric heating systems, *Applied Thermal Engineering* 303 (2026) 131466. https://doi.org/10.1016/j.applthermaleng.2026.131466

[13] F. Fuentes, N. Pailahueque, I. Muñoz, R. Escobar, J.M. Cardemil, Assessing the integration of solar process heat in the dairy industry: A case study in Chile, *Sustainable Energy Technologies and Assessments* 69 (2024) 103894. https://doi.org/10.1016/j.seta.2024.103894

[14] R. Rodríguez Rodrigo, R. Díaz Martín, M. Baranda Fernández, J.A. Román Gallego, C. Mayo del Río, Technical and economic study of solar energy concentration technologies (linear Fresnel and parabolic trough collectors) to generate process heat at medium temperature for the dairy industry of Spain, *Solar Energy* 271 (2024) 112420. https://doi.org/10.1016/j.solener.2024.112420

[15] J. Immonen, K. Mohammadi, K.M. Powell, Simulating a solar parabolic trough collector plant used for industrial process heat using an optimized operating scheme that utilizes flexible heat integration, *Solar Energy* 236 (2022) 756–771. https://doi.org/10.1016/j.solener.2022.03.044

[16] A. Crespo, I. Muñoz, W. Platzer, M. Ibarra, Integration enhancements of a solar parabolic trough system in a Chilean juice industry: Methodology and case study, *Solar Energy* 224 (2021) 593–606. https://doi.org/10.1016/j.solener.2021.03.041

[17] Modelica Association, *Modelica language* https://modelica.org.

[18] Fritzson, P.; Pop, A.; Abdelhak, K.; et al., The OpenModelica integrated environment for modeling, simulation, and model-based development, *Modeling, Identification and Control* 41 (2020) 241–295. https://doi.org/10.4173/mic.2020.4.1.

[19] S. Fahr, D. Tschopp, J.E. Nielsen, K. Kramer, P. Ohnewein, Review of in situ test methods for solar collectors and solar collector arrays, IEA SHC Task 55, Fact Sheet B-D1.2, 2020. https://doi.org/10.18777/ieashc-task55-2020-0014

[20] P. Gilman, A. Dobos, N. DiOrio, J. Freeman, S. Janzou, D. Ryberg, SAM Photovoltaic Model Technical Reference Update, National Renewable Energy Laboratory, Technical Report NREL/TP-6A20-67399, 2018.

[21] Hyundai Energy Solutions, Mono-Crystalline Type HI Series, product datasheet. https://sunwatts.com/content/specs/Hyundai-Green-Energy-HiA-360-385HI-solar-panel-datasheet.pdf (accessed August 2026).

[22] EnergyPlus, EnergyPlus Weather Data, https://energyplus.net/weather (accessed August 2026).

[23] M. Wetter, W. Zuo, T.S. Nouidui, X. Pang, Modelica Buildings library, *Journal of Building Performance Simulation* 7 (4) (2014) 253–270. https://doi.org/10.1080/19401493.2013.765506